Adiabatic hyperspherical representation for the three-body problem in two dimensions

J. P. D'Incao[1,2] and B. D. Esry[2]

[1]*JILA, University of Colorado and NIST, Boulder, Colorado 80309-0440, USA*
[2]*Department of Physics, Kansas State University, Manhattan, Kansas 66506, USA*

We explore the three-body problem in two dimensions using the adiabatic hyperspherical representation. We develop the main equations in terms of democratic hyperangular coordinates and determine several symmetry properties and boundary conditions for both interacting and noninteracting solutions. From the analysis of the three-body effective potentials, we determine the threshold laws for low-energy three-body recombination, collision-induced dissociation, as well as inelastic atom-diatom collisions in two dimensions. Our results show that the hyperspherical representation can offer a simple and conceptually clear physical picture for three-body process in two dimensions which is also suitable for calculations using finite-range two-body interactions supporting a number of bound states.

I. INTRODUCTION

In recent years, ultracold quantum gases have offered the most favorable conditions for exploring universal aspects of few-body physics. Due to the experimental ability to control interatomic interactions using Feshbach resonances [1], the universal few-body physics originated by Efimov [2,3] has become observable and plays an important role in the stability of ultracold quantum gases. Other classes of universal few-body states have also emerged for a variety of unconventional scenarios [3–6], expanding our knowledge of fundamental aspects of few-body systems.

We can further expand our knowledge by considering physics in lower dimensions. In particular, we will consider three-body systems relevant for two-dimensional (2D) ultra-cold gases. Originally, few-body studies in reduced dimensions were motivated by the practical computational benefit. In the case of 2D systems, however, this simplification actually introduces qualitatively different physical properties for the system starting at the two-body level [7,8] with a strong impact on the physics of few-body systems [9–11].

Although the Efimov effect does not occur in 2D [9], a system of three identical bosons interacting via short-range forces has been shown to support universal states [12–20], and a whole new set of few-body states have now emerged [21–25] with the expectation that they will impact several properties of 2D quantum gases. Experimentally, however, it is only possible to create a quasi-2D system, and the connection between such universal states and what can actually be observed experimentally is yet to be determined. Although such experimental conditions can lend themselves to novel physics [26–30], the study of 2D few-body systems provides important knowledge for understanding quasi-2D systems by describing their limiting behavior and should, in part, control the low-energy dependence of scattering observables, i.e., the threshold laws [31–34].

In this paper, we describe the details necessary to implement the adiabatic hyperspherical representation for the three-body problem in 2D. This approach is general and is thus capable of going beyond the usual zero-range model potential used in most of the recent studies of few-body systems in 2D [19–28]. The adiabatic hyperspherical representation offers a simple and conceptually clear description of scattering processes in terms of effective three-body potentials. Here, we explore various symmetry properties and derive boundary conditions that are suitable for numerical calculations with general interactions. Based on our analysis of the long-range behavior of the three-body potentials, we also derive the threshold laws for the three-body scattering observables for ultracold experiments, namely, three-body recombination, collision-induced dissociation, and inelastic atom-diatom collisions.

II. ADIABATIC HYPERSPHERICAL REPRESENTATION

Although different choices of hyperspherical coordinates exist [35], the use of hyperspherical "democratic," or Smith-Whitten, coordinates have proven to be extremely useful for three-atom systems in 3D [36–44]. With this coordinate system, one can conveniently describe all fragmentation channels as well as define the boundary conditions in a manner that is extremely beneficial for numerical implementations.

The motion of three particles in a plane can be described by nearly the same democratic coordinates used in 3D and has been considered at some length by Johnson in Ref. [45]. This is possible since the first step in defining 3D democratic coordinates is going to the body frame, which is always a plane for three bodies. The main difference lies in the description of the Euler angles: in 2D, we need only a single angle. The reduction from three Euler angles in 3D to one in 2D has consequences for the parity and permutation symmetry operations (as we show in Appendix) that, in turn, change the hyperangular boundary conditions from their 3D form.

The 2D democratic coordinates are defined by first transforming the Jacobi vectors $(\vec{\rho}_1, \vec{\rho}_2)$ in the laboratory frame (superscript L) to the body frame via rotation by the Euler angle γ:

$$\begin{pmatrix} \rho_{2x}^L & \rho_{1x}^L \\ \rho_{2y}^L & \rho_{1y}^L \end{pmatrix} = \begin{pmatrix} \cos\gamma & -\sin\gamma \\ \sin\gamma & \cos\gamma \end{pmatrix} \begin{pmatrix} \rho_{2x} & \rho_{1x} \\ \rho_{2y} & \rho_{1y} \end{pmatrix}. \quad (1)$$

In 3D, Eq. (1) would have ρ_{1z}^L and ρ_{2z}^L along with two additional Euler angles in the first matrix on the right-hand side to make it a full 3D rotation matrix, but the body-frame coordinate matrix would not change, i.e., $\rho_{1z} = \rho_{2z} = 0$ [41]. In the above

equation, $\vec{\rho}_1^L$ and $\vec{\rho}_2^L$ are "mass-scaled" Jacobi vectors defined in terms of the individual particle's laboratory-frame positions $\vec{r}_i$ and masses m_i as

$$\vec{\rho}_1^L = (\vec{r}_2 - \vec{r}_1)/d_{12}, \quad \vec{\rho}_2^L = d_{12}\left(\vec{r}_3 - \frac{m_1\vec{r}_1 + m_2\vec{r}_2}{m_1 + m_2}\right), \quad (2)$$

with

$$\mu d_{ij}^2 = \frac{m_k(m_i + m_j)}{m_1 + m_2 + m_3} \quad \text{and} \quad \mu^2 = \frac{m_1 m_2 m_3}{m_1 + m_2 + m_3}, \quad (3)$$

where the indices (i,j,k) are a cyclic permutation of $(1,2,3)$ and μ is the three-body reduced mass. Note that the choice of μ is arbitrary, but the present choice ensures that the volume element remains independent of mass [46].

The hyperangles are defined by the condition that the moment of inertia tensor is diagonal [45], which is accomplished by the transformation

$$\begin{pmatrix} \rho_{2x} & \rho_{1x} \\ \rho_{2y} & \rho_{1y} \end{pmatrix} = R\begin{pmatrix} \cos\theta' & 0 \\ 0 & \sin\theta' \end{pmatrix}\begin{pmatrix} \cos\varphi' & \sin\varphi' \\ -\sin\varphi' & \cos\varphi' \end{pmatrix}. \quad (4)$$

Here, $\theta' = \theta/2 - \pi/4$ and $\varphi' = \varphi/2 + \pi/6$, with θ and φ being the democratic hyperangles describing the internal motion of the particles, and

$$R = (\rho_1^2 + \rho_2^2)^{1/2} \quad (5)$$

is the hyperradius giving the overall size of the system. The hyperspherical coordinates are defined within the ranges

$$\begin{aligned} 0 \leqslant R < \infty, \quad & 0 \leqslant \theta \leqslant \pi, \\ 0 \leqslant \varphi \leqslant 4\pi, \quad & 0 \leqslant \gamma \leqslant 2\pi. \end{aligned} \quad (6)$$

Besides the single Euler angle, the main difference between the 2D and 3D definitions of these coordinates is the range of θ. In 3D, θ only takes on values between 0 and $\frac{\pi}{2}$. The change in going to 2D comes from the fact that there is no Euler angle that can change the orientation of the body-frame z axis. In 3D, the orientation of the z axis is determined by $\vec{\rho}_1^L \times \vec{\rho}_2^L$ and is thus a dynamical quantity. In 2D, the z axis is fixed. More precisely, the plane of the particles is fixed and thus contains all configurations of the particles, i.e., both signs of $\vec{\rho}_1^L \times \vec{\rho}_2^L$. Consequently, the range of θ is doubled to correctly reproduce all configurations of the particles. We will further see in Appendix that θ is affected by permutations while it is not in 3D [42–44].

With the definitions above, we can now introduce the three-body Schrödinger equation in 2D for the rescaled total wave function $\Psi \to \Psi/R^{3/2}$ (atomic units will be used unless otherwise noted),

$$\left[-\frac{1}{2\mu}\frac{\partial^2}{\partial R^2} + H_{\text{ad}}(R,\Omega)\right]\Psi(R,\Omega) = E\Psi(R,\Omega), \quad (7)$$

where E is the total energy and $\Omega \equiv \{\theta,\varphi,\gamma\}$ denotes the set of all hyperangles. In Eq. (7), the adiabatic Hamiltonian is given by

$$H_{\text{ad}}(R,\Omega) = \frac{\Lambda^2(\Omega) + 3/4}{2\mu R^2} + V(R,\theta,\varphi), \quad (8)$$

containing the grand angular momentum, i.e., the hyperangular part of the kinetic energy,

$$\begin{aligned} \Lambda^2(\Omega) = &-4\left(\frac{1}{\sin\theta}\frac{\partial}{\partial\theta}\sin\theta\frac{\partial}{\partial\theta} + \frac{1}{\sin^2\theta}\frac{\partial^2}{\partial\varphi^2}\right) \\ &- \frac{1}{\sin^2\theta}\left(\frac{\partial^2}{\partial\gamma^2} - 4\cos\theta\frac{\partial^2}{\partial\gamma\,\partial\varphi}\right), \end{aligned}$$

as well as all the interparticle interactions via $V(R,\theta,\varphi)$. The grand angular momentum operator is essentially the same as in 3D save for a few factors of 2 [41] and, of course, the Euler angles.

Although it is not necessary, we typically assume the interactions to be a pairwise sum of the form

$$V(R,\theta,\varphi) = v(r_{12}) + v(r_{23}) + v(r_{31}), \quad (9)$$

where the interparticle distances r_{ij} are given in terms of the hyperspherical coordinates by

$$\begin{aligned} r_{12} &= 2^{-1/2}d_{12}R\,[1 + \sin\theta\cos(\varphi + \varphi_{12})]^{1/2}, \\ r_{23} &= 2^{-1/2}d_{23}R\,[1 + \sin\theta\cos(\varphi + \varphi_{23})]^{1/2}, \quad (10) \\ r_{31} &= 2^{-1/2}d_{31}R\,[1 + \sin\theta\cos(\varphi + \varphi_{31})]^{1/2}. \end{aligned}$$

The mass-dependent angles are $\varphi_{12} = 2\tan^{-1}(m_3/\mu)$, $\varphi_{23} = 0$, and $\varphi_{31} = -2\tan^{-1}(m_2/\mu)$. Nonadditive forces be can easily introduced in Eq. (9) with effectively no cost to the calculations [47].

It should be noted that the wave function must satisfy the condition

$$\Psi(R,\theta,\varphi + 2\pi,\gamma + \pi) = \Psi(R,\theta,\varphi,\gamma) \quad (11)$$

to ensure that the wave function is single valued.

In the adiabatic hyperspherical representation, the total wave function is expanded in terms of the channel functions $\Phi_\nu(R;\Omega)$,

$$\Psi(R,\Omega) = \sum_\nu F_\nu(R)\Phi_\nu(R;\Omega), \quad (12)$$

where $F_\nu(R)$ are the hyperradial wave functions and ν represents all quantum numbers necessary to specify each channel. The channel functions $\Phi_\nu(R;\Omega)$ form a complete set of orthonormal functions at each value of R and are eigenfunctions of H_{ad},

$$H_{\text{ad}}(R,\Omega)\Phi_\nu(R;\Omega) = U_\nu(R)\Phi_\nu(R;\Omega). \quad (13)$$

The eigenvalues $U_\nu(R)$ are the three-body potentials from which, as we will see next, one can define *effective* three-body potentials for the hyperradial motion.

Substituting Eq. (12) into the Schrödinger equation (7) and projecting out $\Phi_{\nu'}$ (the volume element in 2D is $dR\sin\theta\,d\theta\,d\varphi\,d\gamma/4$ [45]), we obtain the hyperradial Schrödinger equation

$$\begin{aligned} \left[-\frac{1}{2\mu}\frac{d^2}{dR^2} + W_\nu(R)\right]F_\nu(R) &- \frac{1}{2\mu}\sum_{\nu'\neq\nu}\left[P_{\nu\nu'}(R)\frac{d}{dR}\right. \\ &\left. + \frac{d}{dR}P_{\nu\nu'}(R) + Q_{\nu\nu'}(R)\right]F_{\nu'}(R) = EF_\nu(R), \quad (14) \end{aligned}$$

that describes the motion of the three-body system under the influence of the effective potentials

$$W_\nu(R) = U_\nu(R) - \frac{Q_{\nu\nu}(R)}{2\mu}. \tag{15}$$

As we will see in Sec. V, including $Q_{\nu\nu}(R)$ in the definition of the effective potential $W_\nu(R)$ is crucial for obtaining potentials with the correct behavior at large distances. In the adiabatic hyperspherical representation, the nonadiabatic coupling terms $P_{\nu\nu'}(R)$ and $Q_{\nu\nu'}(R)$ ($\nu \neq \nu'$) drive inelastic collisions and are defined as

$$P_{\nu\nu'}(R) = \left\langle\!\!\left\langle \Phi_\nu \left| \frac{d\Phi_{\nu'}}{dR} \right. \right\rangle\!\!\right\rangle \tag{16}$$

and

$$Q_{\nu\nu'}(R) = \left\langle\!\!\left\langle \frac{d\Phi_\nu}{dR} \left| \frac{d\Phi_{\nu'}}{dR} \right. \right\rangle\!\!\right\rangle. \tag{17}$$

The double brackets denote integration over the angular coordinates Ω only. As it stands, Eq. (14) is exact. In practice, of course, the sum over channels must be truncated and the number of channels retained increased until one achieves the desired accuracy.

III. SYMMETRIZED HYPERSPHERICAL HARMONICS

To quickly assess the symmetry properties and degeneracy that are important for the large-R behavior where interactions are negligible, we analyze the 2D noninteracting [$V(R,\theta,\varphi) = 0$ in Eq. (8)] solutions, i.e., the hyperspherical harmonics. The symmetrized hyperspherical harmonics derived here will, of course, also satisfy the boundary conditions we derive in Sec. IV. They thus serve as a confirmation of those findings.

One interesting property of the three-body problem in 2D, unlike the 3D case, is that the hyperspherical harmonics can be written in closed form

$$\Lambda^2 Y_{\omega M}^\lambda(\Omega) = \lambda(\lambda + 2)Y_{\omega M}^\lambda(\Omega), \tag{18}$$

with Y being defined in terms of the Wigner d-function as

$$Y_{\omega M}^\lambda(\Omega) = \frac{1}{\pi}\sqrt{\frac{\lambda + 1}{4}} e^{i\frac{\omega}{2}\varphi} d_{\frac{\omega}{2}\frac{M}{2}}^{\frac{\lambda}{2}}(\theta) e^{iM\gamma}. \tag{19}$$

Here, λ is the hyperangular momentum quantum number, ω is a quantum number labeling degenerate eigenstates, and M is the total orbital angular momentum. Note that the condition in Eq. (11) and the fact that $-\lambda \leqslant \{\omega, M\} \leqslant \lambda$ (from the properties of the Wigner d-functions) imply that λ, ω, and M must all be either even or odd integers. This condition is satisfied if these quantum numbers, specifically $\lambda/2$, $\omega/2$, and $M/2$, obey the usual rules for angular momenta if ω and M are regarded as projections of λ.

With this closed form for the hyperspherical harmonics, we can explore the allowed quantum numbers for a given permutation symmetry when the three-body system has indistinguishable particles. The idea is to determine the effects of the coordinate transformations due to parity Π and to permutations of particles i and j (P_{ij}) on these analytic functions. This analysis is outlined in Appendix and

summarized here:

$$\Pi Y_{\omega M}^\lambda(\Omega) = (-1)^M Y_{\omega M}^\lambda(\Omega), \tag{20}$$

$$P_{12} Y_{\omega M}^\lambda(\Omega) = (-1)^{\frac{M+\lambda}{2}} e^{-i\omega\frac{\pi}{3}} Y_{-\omega M}^\lambda(\Omega), \tag{21}$$

$$P_{23} Y_{\omega M}^\lambda(\Omega) = (-1)^{\frac{M+\lambda}{2}} e^{i\omega\frac{\pi}{3}} Y_{-\omega M}^\lambda(\Omega), \tag{22}$$

$$P_{31} Y_{\omega M}^\lambda(\Omega) = (-1)^{\frac{M+\lambda}{2}} e^{i\omega\pi} Y_{-\omega M}^\lambda(\Omega), \tag{23}$$

$$P_{12} P_{23} Y_{\omega M}^\lambda(\Omega) = e^{i\omega\frac{2\pi}{3}} Y_{\omega M}^\lambda(\Omega), \tag{24}$$

$$P_{12} P_{31} Y_{\omega M}^\lambda(\Omega) = e^{-i\omega\frac{2\pi}{3}} Y_{\omega M}^\lambda(\Omega). \tag{25}$$

Note that the hyperradius is invariant under all the symmetry operations above. Note also that in the derivation of Eqs. (20)–(25) the only nontrivial relation used was that the d function in Eq. (19) has the following property: $d_{mm'}^\ell(\pi - \theta) = (-1)^{\ell+m'} d_{-mm'}^\ell(\theta)$. As one can see, the hyperspherical harmonics are already parity eigenstates. Since M is the total orbital angular momentum and is thus a good quantum number, none of the permutation operators change M. The symmetrized harmonics we will construct based on Eqs. (20)–(25) will thus remain parity eigenstates. Note also that our derivation of the symmetrized harmonics below assumes that the spin part of the total wave function is symmetric under permutation. As a result, we only need to impose permutation symmetry on the spatial part of the wave function represented here by the hyperspherical harmonics.

A. Three identical bosons

For three identical bosons (BBB), we are interested in the completely symmetric hyperspherical harmonics. To obtain these states, we apply the (un-normalized) symmetrization operator $\mathcal{S} = (1 + P_{12} + P_{23} + P_{31} + P_{12}P_{23} + P_{12}P_{31})$ to the hyperspherical harmonics defined in Eq. (19) and use Eqs. (20)–(25). Doing so, we find

$$\begin{aligned} \mathcal{S} Y_{\omega M}^\lambda(\Omega) &= [1 + (-1)^M e^{i\omega\frac{\pi}{3}} + e^{i\omega\frac{2\pi}{3}}] \\ &\times \left[Y_{\omega M}^\lambda(\Omega) + (-1)^{\frac{3M+\lambda}{2}} Y_{-\omega M}^\lambda(\Omega) \right]. \end{aligned} \tag{26}$$

The prefactor here should not vanish. This condition determines, for a given value of M, the allowed values for λ and ω. By inspection, we find that we must have

$$\omega = \begin{cases} 6n, & M \text{ even} \\ 6n + 3, & M \text{ odd}. \end{cases} \quad (n = 0,1,2,\ldots). \tag{27}$$

Note that these conditions are essentially what we found for the 3D case [41]. Now, we recall from Eq. (11) that λ, ω, and M must all be even or odd. Equation (26) further tells us that if $\frac{3M+\lambda}{2}$ is odd, then ω cannot be zero or the function will vanish. But, ω can only be zero if M is even. So, we amend Eq. (27) to

$$\omega = \begin{cases} 6n, & (n \neq 0 \text{ if } \frac{3M+\lambda}{2} \text{ odd}), M \text{ even} \\ 6n + 3, & M \text{ odd}. \end{cases} \tag{28}$$

Explicit examples for the allowed quantum numbers are given in Table I for the lowest few values of M.

TABLE I. Sample of allowed hyperspherical harmonic quantum numbers for three identical bosons (BBB). We list the lowest few values for both λ and M.

$M = 0$		$|M| = 1$		$|M| = 2$		$|M| = 3$	
λ	$|\omega|$	λ	$|\omega|$	λ	$|\omega|$	λ	$|\omega|$
0	0	3	3	2	0	3	3
4	0	5	3	6	0,6	5	3
6	6	7	3	8	6	7	3
8	0,6	9	3,9	10	0,6	9	3,9

B. Three identical fermions

For three identical fermions (FFF), we are interested in the completely antisymmetric hyperspherical harmonics. So, we now apply the antisymmetrization operator $\mathcal{A} = (1 - P_{12} - P_{23} - P_{31} + P_{12}P_{23} + P_{12}P_{31})$ to Eq. (19) and find

$$\mathcal{A}Y_{\omega M}^{\lambda}(\Omega) = [1 + (-1)^M e^{i\omega\frac{\pi}{3}} + e^{i\omega\frac{2\pi}{3}}]$$
$$\times [Y_{\omega M}^{\lambda}(\Omega) - (-1)^{\frac{3M+\lambda}{2}} Y_{-\omega M}^{\lambda}(\Omega)]. \quad (29)$$

Just as for the bosons, the prefactor here should not vanish, so we must have

$$\omega = \begin{cases} 6n, & M \text{ even} \\ 6n + 3, & M \text{ odd.} \end{cases} \quad (30)$$

These conditions are exactly the same as for bosons. The difference due to antisymmetry stems from the fact that $\frac{3M+\lambda}{2}$ must be odd when $\omega = 0$ or the function will vanish (opposite the case for bosons). But, ω can only be zero if M is even, so $\lambda/2$ must be *odd*. So, we qualify Eq. (30) as

$$\omega = \begin{cases} 6n, & (n \neq 0 \text{ if } \frac{3M+\lambda}{2} \text{ even}), M \text{ even} \\ 6n + 3, & M \text{ odd.} \end{cases} \quad (31)$$

Explicit examples are given in Table II.

C. Two identical bosons

When there are only two identical bosons (BBX) and they are labeled 1 and 3, we symmetrize the hyperspherical harmonics by applying $\mathcal{S} = (1 + P_{31})$ to Eq. (19). In this case, symmetrization for bosons requires

$$\mathcal{S}Y_{\omega M}^{\lambda}(\Omega) = Y_{\omega M}^{\lambda}(\Omega) + (-1)^{\frac{3M+\lambda}{2}} Y_{-\omega M}^{\lambda}(\Omega). \quad (32)$$

There are thus no restrictions on ω except that $\omega \neq 0$ if $\frac{3M+\lambda}{2}$ is odd. Some of the allowed λ and ω are given in Table III.

TABLE III. Same as Table I but for two identical bosons (BBX).

$M = 0$		$|M| = 1$		$|M| = 2$		$|M| = 3$	
λ	$|\omega|$	λ	$|\omega|$	λ	$|\omega|$	λ	$|\omega|$
0	0	1	1	2	0,2	3	1,3
2	2	3	1,3	4	2,4	5	1,3,5
4	0,2,4	5	1,3,5	6	0,2,4,6	7	1,3,5,7
6	2,4,6	7	1,3,5,7	8	2,4,6,8	9	1,3,5,7,9

D. Two identical fermions

To complete our analysis, we consider the case of two identical fermions (FFX), i.e. applying $\mathcal{A} = (1 - P_{31})$ to Eq. (19). For this case, we find

$$\mathcal{A}Y_{\omega M}^{\lambda}(\Omega) = Y_{\omega M}^{\lambda}(\Omega) - (-1)^{\frac{3M+\lambda}{2}} Y_{-\omega M}^{\lambda}(\Omega). \quad (33)$$

Again, there are no restrictions on ω except that $\omega \neq 0$ if $\frac{3M+\lambda}{2}$ is now even. Some of the allowed λ and ω are given in Table IV.

IV. BOUNDARY CONDITIONS

While the symmetrized harmonics of Sec. III can be used as a basis to expand Φ_ν and solve Eq. (13), they are an inefficient choice in practice. The difficulty with this basis is due to the localization of Φ_ν in the hyperangular plane as R increases, requiring the number of basis functions to grow. Specifically, a simple uncertainty argument shows that their number must grow at least linearly with R in order to describe the localized two-body channels. More flexible methods such as b-splines or finite elements have proven much more effective [41]. Symmetries must still be imposed, however, and can actually improve these methods' efficiency by reducing the required integration domain. This reduction is accomplished by imposing boundary conditions on the smallest unique region the symmetry allows. For instance, three identical particles permits a reduction of the integration domain by 3! [41].

In this section, we will derive these boundary conditions. Although the analysis in the previous section already gives the information necessary for obtaining the boundary conditions, we will take an alternative, independent approach here. The results, of course, are equivalent. Note that since the hyperradius is invariant under symmetry operations in Eqs. (20)–(25), symmetry-motivated boundary conditions need only be imposed in the hyperangles.

For isotropic two-body interactions, such that M is a good quantum number, the channel functions are separable in the

TABLE II. Same as Table I but for three identical fermions (FFF).

$M = 0$		$|M| = 1$		$|M| = 2$		$|M| = 3$	
λ	$|\omega|$	λ	$|\omega|$	λ	$|\omega|$	λ	$|\omega|$
2	0	3	3	4	0	3	3
6	0,6	5	3	6	6	5	3
8	6	7	3	8	0,6	7	3
10	0,6	9	3,9	10	6	9	3,9

TABLE IV. Same as Table I but for two identical fermions (FFX).

$M = 0$		$|M| = 1$		$|M| = 2$		$|M| = 3$	
λ	$|\omega|$	λ	$|\omega|$	λ	$|\omega|$	λ	$|\omega|$
2	0,2	1	1	2	2	3	1,3
4	2,4	3	1,3	4	0,2,4	5	1,3,5
6	0,2,4,6	5	1,3,5	6	2,4,6	7	1,3,5,7
8	2,4,6,8	7	1,3,5,7	8	0,2,4,6,8	9	1,3,5,7,9

Euler angle γ, with the corresponding solution normally expressed by $\exp(iM\gamma)$. As a result, Φ_ν is an eigenstate of $L_z = i\partial/\partial\gamma$. In this basis, however, the adiabatic Schrödinger equation (13) is complex and the boundary conditions are difficult to implement. As we will show in the following, a change of basis to $\sin(M\gamma)$ and $\cos(M\gamma)$,

$$\Phi(R;\Omega) = \phi_s(R;\theta,\varphi)\sin M\gamma + \phi_c(R;\theta,\varphi)\cos M\gamma,$$
(34)

transforms the adiabatic equation into a real system of equations

$$\left[-4\left(\frac{1}{\sin\theta}\frac{\partial}{\partial\theta}\sin\theta\frac{\partial}{\partial\theta} + \frac{1}{\sin^2\theta}\frac{\partial^2}{\partial\varphi^2} \right) + \frac{M^2}{\sin^2\theta} \right]\begin{pmatrix}\phi_s \\ \phi_c\end{pmatrix}$$
$$+ 4\frac{\cos\theta}{\sin^2\theta}M\frac{\partial}{\partial\varphi}\begin{pmatrix}-\phi_c \\ \phi_s\end{pmatrix} = 2\mu R^2 U(R)\begin{pmatrix}\phi_s \\ \phi_c\end{pmatrix},$$
(35)

where each component ϕ_s and ϕ_c will have its own set of boundary conditions, making this basis more convenient computationally. This choice, of course, also implies that Φ_ν is an eigenstate of L_z^2 rather than of L_z.

A. Reflection symmetry

We start the present analysis by first noting that, besides the symmetry operations in Eqs. (20)–(25) (see also Appendix), H_{ad} is invariant under the operations

$$R_x : (\theta,\varphi,\gamma) \rightarrow (\pi - \theta,\varphi,2\pi - \gamma),$$
(36)

$$R_y : (\theta,\varphi,\gamma) \rightarrow (\pi - \theta,\varphi,\pi - \gamma),$$
(37)

where R_x and R_y are reflections along the body-frame x and y axes, respectively, as can be verified by applying the above transformations in Eq. (4). Since H_{ad} commutes with R_x and R_y, they can share common eigenstates. Therefore, the solutions of H_{ad}, i.e., the channel functions Φ_ν in Eq. (13), can be chosen to obey the boundary conditions resulting from these reflections. We note, however, that since $R_x R_y = \Pi$ we only need to specify the boundary conditions with respect to one of the reflections, which we arbitrarily choose to be R_x. We also note that the $\sin(M\gamma)$ and $\cos(M\gamma)$ functions in Eq. (34) are eigenstates of R_x (R_y) with eigenvalues -1 $(+1)$ and $+1$ (-1), respectively, while $\exp(iM\gamma)$ is not. Expressing Φ_ν as in Eq. (34), we have thus chosen to construct eigenstates of $\{H_{\mathrm{ad}},\Pi,L_z^2,R_x\}$ instead of $\{H_{\mathrm{ad}},\Pi,L_z\}$, purely for our computational convenience. Three-body states are thus labeled by $|M|_r^\pi$ where r indicates the R_x symmetry as defined below.

Now, in order to establish the boundary conditions due to R_x, we recognize that the channel functions, irrespective of the system's permutation symmetry, can only be symmetric or antisymmetric with respect to reflections. This allows us to write

$$R_x\Phi(R;\Omega) = (-1)^r\Phi(R;\Omega),$$
(38)

where $r = 0$ for symmetric solutions and $r = 1$ for antisymmetric solutions. Moreover, since R_x [Eq. (36)] keeps φ unchanged, the boundary conditions due to reflections will only affect θ. Substituting Eq. (34) into Eq. (38) and projecting

out $\sin(M\gamma)$ and $\cos(M\gamma)$, we obtain

$$\phi_s(R;\pi - \theta,\varphi) = (-1)^{r+1}\phi_s(R;\theta,\varphi),$$
(39)

$$\phi_c(R;\pi - \theta,\varphi) = (-1)^r\phi_c(R;\theta,\varphi)$$
(40)

and

$$\frac{\partial}{\partial\theta}\phi_s(R;\pi - \theta,\varphi) = (-1)^r\frac{\partial}{\partial\theta}\phi_s(R;\theta,\varphi),$$
(41)

$$\frac{\partial}{\partial\theta}\phi_c(R;\pi - \theta,\varphi) = (-1)^{r+1}\frac{\partial}{\partial\theta}\phi_c(R;\theta,\varphi).$$
(42)

Equations (39)–(42) imply that ϕ_s and ϕ_c are either even or odd upon reflection through $\theta = \pi/2$. We can thus extract the following boundary conditions at $\theta = \pi/2$. For symmetric solutions ($r = 0$),

$$\phi_s\left(R,\frac{\pi}{2},\varphi\right) = 0 \quad \text{and} \quad \left.\frac{\partial}{\partial\theta}\phi_c(R;\theta,\varphi)\right|_{\theta=\frac{\pi}{2}} = 0. \quad (43)$$

For antisymmetric solutions ($r = 1$), the boundary conditions are:

$$\left.\frac{\partial}{\partial\theta}\phi_s(R;\theta,\varphi)\right|_{\theta=\frac{\pi}{2}} = 0 \quad \text{and} \quad \phi_c\left(R,\frac{\pi}{2},\varphi\right) = 0. \quad (44)$$

Since the volume element vanishes at $\theta = 0$, no boundary condition is required. The integration domain has thus been reduced to $0 \leqslant \theta \leqslant \pi/2$, thereby reducing the numerical effort by a factor of 2.

B. Permutation symmetry

The boundary conditions in φ originate from the permutation symmetry, i.e., they will depend on the bosonic or fermionic character of the three particles. As we will see, however, the reflection symmetry [Eqs. (39) and (40)], as well as the condition in Eq. (11), will also be used in deriving the boundary conditions in φ.

Because we assume the atoms are in a spin-stretched state, i.e., the spin part of the wave function is symmetric under permutations, the bosonic or fermionic symmetry must be satisfied by the spatial part of the wave function. In fact, the boundary conditions for the channel functions are derived from the requirement that they must have a well-defined permutation symmetry, namely,

$$P_{ij}\Phi(R;\Omega) = (-1)^s\Phi(R;\Omega).$$
(45)

In the above equation, $s = 0$ for a pair of identical bosons while $s = 1$ for identical fermions. Two dissimilar particles require no such condition. Otherwise, the derivation of the boundary conditions in φ follows closely, in spirit, to the θ-boundary-condition derivation in the previous section.

1. Three identical particles

Although there exists a total of five possible permutations of three particles, i.e., P_{12}, P_{23}, P_{31}, $P_{12}P_{23}$, and $P_{12}P_{31}$, we only need to symmetrize with respect to two of them (see Appendix). This simplification follows from the fact that the S_3 permutation group has only two generators so that all permutations can be written as products of any two permutations [48]. We will, therefore, choose P_{31} and P_{23} as

generators and derive the boundary conditions based on these operations.

Since we expect a 3! reduction in the integration domain, we will seek boundary conditions at $\varphi = 0$ and $\pi/3$ [Eq. (11) already reduced the range of φ from Eq. (6) to $0 \leqslant \varphi \leqslant 2\pi$]. So, substituting Φ from Eq. (34) into Eq. (45), using $P_{31}(\theta,\varphi,\gamma) = (\pi - \theta, 2\pi - \varphi, \gamma)$ from Eq. (A15), and projecting out $\sin(M\gamma)$ and $\cos(M\gamma)$, we obtain at $\varphi = 0$

$$\phi_s(R;\theta,0) = (-1)^{r+s+M+1}\phi_s(R;\theta,0), \tag{46}$$

$$\phi_c(R;\theta,0) = (-1)^{r+s+M}\phi_c(R;\theta,0) \tag{47}$$

and

$$\frac{\partial}{\partial\varphi}\phi_s(R;\theta,\varphi)\bigg|_{\varphi=0} = (-1)^{r+s+M}\frac{\partial}{\partial\varphi}\phi_s(R;\theta,\varphi)\bigg|_{\varphi=0}, \tag{48}$$

$$\frac{\partial}{\partial\varphi}\phi_c(R;\theta,\varphi)\bigg|_{\varphi=0} = (-1)^{r+s+M+1}\frac{\partial}{\partial\varphi}\phi_c(R;\theta,\varphi)\bigg|_{\varphi=0}. \tag{49}$$

We note that to obtain Eqs. (46)–(49) we used Eqs. (39) and (40) which introduced the dependence on r, as well as Eq. (11), which introduced the dependence on M.

For $\varphi = \pi/3$, we similarly use Eqs. (A13) and (A14), $P_{23}(\theta,\varphi,\gamma) = (\pi - \theta, 2\pi/3 - \varphi, \gamma)$, to obtain the following conditions,

$$\phi_s\left(R;\theta,\frac{\pi}{3}\right) = (-1)^{r+s+1}\phi_s\left(R;\theta,\frac{\pi}{3}\right), \tag{50}$$

$$\phi_c\left(R;\theta,\frac{\pi}{3}\right) = (-1)^{r+s}\phi_c\left(R;\theta,\frac{\pi}{3}\right) \tag{51}$$

and

$$\frac{\partial}{\partial\varphi}\phi_s(R;\theta,\varphi)\bigg|_{\varphi=\frac{\pi}{3}} = (-1)^{r+s}\frac{\partial}{\partial\varphi}\phi_s(R;\theta,\varphi)\bigg|_{\varphi=\frac{\pi}{3}}, \tag{52}$$

$$\frac{\partial}{\partial\varphi}\phi_c(R;\theta,\varphi)\bigg|_{\varphi=\frac{\pi}{3}} = (-1)^{r+s+1}\frac{\partial}{\partial\varphi}\phi_c(R;\theta,\varphi)\bigg|_{\varphi=\frac{\pi}{3}}. \tag{53}$$

Therefore, we need only integrate Eq. (13) from $\varphi = 0$ to $\pi/3$, making the integration domain a factor of 6 smaller. Note that, similar to the boundary conditions in θ, Eqs. (50)–(53) finally only require ϕ_s and ϕ_c, or their derivative, to vanish and are thus relatively simple to implement in practice.

2. Two identical particles

For systems with only two identical particles, the determination of the boundary conditions is simpler since the channel function must be symmetrized for only a single permutation. Here, we will assume that particles 1 and 3 are identical such that the relevant permutation is P_{31}, leading us to seek boundary conditions at $\varphi = 0$ and π. Therefore, proceeding as in Sec. IVB1, substituting Φ into (45), where $P_{31}(\theta,\varphi,\gamma) = (\pi - \theta, 2\pi - \varphi, \gamma)$ from Eq. (A15), and projecting out $\sin(M\gamma)$ and $\cos(M\gamma)$, we obtain at $\varphi = 0$

$$\phi_s(R;\theta,0) = (-1)^{r+s+M+1}\phi_s(R;\theta,0), \tag{54}$$

$$\phi_c(R;\theta,0) = (-1)^{r+s+M}\phi_c(R;\theta,0) \tag{55}$$

TABLE V. Summary of the boundary conditions for bosonic (BBB and BBX) and fermionic (FFF and FFX) systems. The table indicates the relevant quantum number for permutation (s) and reflection (r) symmetry. The boundary conditions at $\theta = 0$, $\varphi = 0$, and $\varphi = \pi/3$ (for BBB and FFF) or π (for BBX and FFX) specify whether the components ϕ_s and ϕ_c of Φ, or their derivative, vanishes ($\partial_\theta = \partial/\partial\theta$ and $\partial_\varphi = \partial/\partial\varphi$).

		BBB or BBX ($s=0$)		
r	M	$\theta = \pi/2$	$\varphi = 0$	$\varphi = \pi/3$ or π
0	even	$\{\phi_s, \partial_\theta\phi_c\} = 0$	$\{\phi_s, \partial_\varphi\phi_c\} = 0$	$\{\phi_s, \partial_\varphi\phi_c\} = 0$
	odd	$\{\phi_s, \partial_\theta\phi_c\} = 0$	$\{\partial_\varphi\phi_s, \phi_c\} = 0$	$\{\phi_s, \partial_\varphi\phi_c\} = 0$
1	even	$\{\partial_\theta\phi_s, \phi_c\} = 0$	$\{\partial_\varphi\phi_s, \phi_c\} = 0$	$\{\partial_\varphi\phi_s, \phi_c\} = 0$
	odd	$\{\partial_\theta\phi_s, \phi_c\} = 0$	$\{\phi_s, \partial_\varphi\phi_c\} = 0$	$\{\partial_\varphi\phi_s, \phi_c\} = 0$
		FFF or FFX ($s=1$)		
r	M	$\theta = \pi/2$	$\varphi = 0$	$\varphi = \pi/3$ or π
0	even	$\{\phi_s, \partial_\theta\phi_c\} = 0$	$\{\partial_\varphi\phi_s, \phi_c\} = 0$	$\{\partial_\varphi\phi_s, \phi_c\} = 0$
	odd	$\{\phi_s, \partial_\theta\phi_c\} = 0$	$\{\phi_s, \partial_\varphi\phi_c\} = 0$	$\{\partial_\varphi\phi_s, \phi_c\} = 0$
1	even	$\{\partial_\theta\phi_s, \phi_c\} = 0$	$\{\phi_s, \partial_\varphi\phi_c\} = 0$	$\{\phi_s, \partial_\varphi\phi_c\} = 0$
	odd	$\{\partial_\theta\phi_s, \phi_c\} = 0$	$\{\partial_\varphi\phi_s, \phi_c\} = 0$	$\{\phi_s, \partial_\varphi\phi_c\} = 0$

and

$$\frac{\partial}{\partial\varphi}\phi_s(R;\theta,\varphi)\bigg|_{\varphi=0} = (-1)^{r+s+M}\frac{\partial}{\partial\varphi}\phi_s(R;\theta,\varphi)\bigg|_{\varphi=0}, \tag{56}$$

$$\frac{\partial}{\partial\varphi}\phi_c(R;\theta,\varphi)\bigg|_{\varphi=0} = (-1)^{r+s+M+1}\frac{\partial}{\partial\varphi}\phi_c(R;\theta,\varphi)\bigg|_{\varphi=0}. \tag{57}$$

These boundary conditions are identical to Eqs. (46)–(49).

To obtain the other set of boundary conditions, we repeat the process above without imposing the condition in Eq. (11). This yields the following conditions at $\varphi = \pi$,

$$\phi_s(R;\theta,\pi) = (-1)^{r+s+1}\phi_s(R;\theta,\pi), \tag{58}$$

$$\phi_c(R;\theta,\pi) = (-1)^{r+s}\phi_c(R;\theta,\pi) \tag{59}$$

and

$$\frac{\partial}{\partial\varphi}\phi_s(R;\theta,\varphi)\bigg|_{\varphi=\pi} = (-1)^{r+s}\frac{\partial}{\partial\varphi}\phi_s(R;\theta,\varphi)\bigg|_{\varphi=\pi}, \tag{60}$$

$$\frac{\partial}{\partial\varphi}\phi_c(R;\theta,\varphi)\bigg|_{\varphi=\pi} = (-1)^{r+s+1}\frac{\partial}{\partial\varphi}\phi_c(R;\theta,\varphi)\bigg|_{\varphi=\pi}. \tag{61}$$

The boundary conditions above have the same form as Eqs. (50)–(53) but are evaluated at $\varphi = \pi$ instead of $\pi/3$. Therefore, for systems with two identical particles we need only to integrate Eq. (13) from $\varphi = 0$ to π, reducing the integration domain by a factor of 2.

In Table V, we summarize all the boundary conditions derived in this section for systems with three identical particles (BBB and FFF) as well as for systems with two identical particles (BBX and FFX).

3. Three distinguishable particles

For three distinguishable particles, of course, no permutational symmetry is required, resulting in no boundary conditions in φ. The only boundary condition in φ is the one provided by Eq. (11) for the one-to-one correspondence of the

wave function in the body and laboratory frames. This results in periodic boundary conditions for the channel functions, and their derivative, given by

$$\phi_s(R;\theta,0) = (-1)^M \phi_s(R;\theta,2\pi),\qquad(62)$$

$$\phi_c(R;\theta,0) = (-1)^M \phi_c(R;\theta,2\pi),\qquad(63)$$

$$\frac{\partial}{\partial\varphi}\phi_s(R;\theta,\varphi)\bigg|_{\varphi=0} = (-1)^{M+1}\frac{\partial}{\partial\varphi}\phi_s(R;\theta,\varphi)\bigg|_{\varphi=2\pi},\quad(64)$$

$$\frac{\partial}{\partial\varphi}\phi_c(R;\theta,\varphi)\bigg|_{\varphi=0} = (-1)^{M+1}\frac{\partial}{\partial\varphi}\phi_c(R;\theta,\varphi)\bigg|_{\varphi=2\pi}.\quad(65)$$

For this case, therefore, the only reduction in the integration domain in Eq. (6) is provided by the reflection symmetry which reduces the range in θ by a factor of 2.

V. STRUCTURE OF THE THREE-BODY POTENTIALS IN 2D

One of the advantages of the adiabatic hyperspherical representation is that besides producing numerically accurate results, it also offers a simple and conceptually clear description of the system in terms of the three-body potentials $U_\nu(R)$. The three-body potentials are obtained by solving the adiabatic equation (13) for fixed values of R. Once this step is completed, one can solve the hyperradial Schrödinger equation (14) to obtain the three-body bound and scattering states from which any three-body observable can be computed.

A. Numerical details

For 2D three-body systems, we must thus solve the two coupled partial differential equations in θ and φ (one for $M = 0$) in Eq. (35). The resulting differential equations are solved by expanding ϕ_s and ϕ_c in Eq. (34) onto a direct product of

basis splines [49], in the same spirit as the 3D three-body problem [41], with the boundary conditions shown in Table V. Here, we used 50 basis splines for each direction in the θ-φ hyperangular plane and obtained at least six digits of accuracy for the potentials U_ν for values of R up to $10r_0$. As usual, we used a nonuniform grid distribution, concentrating more points near the potential minima where the channel functions change more drastically. The grid distribution and the number of points depends on the behavior of the interaction potential. The values quoted above are specific to our assumed form [Eq. (66)] for the two-body potential. Its lack of a strong repulsive core facilitates the numerical calculations without impacting the universality of the results.

In what follows, we will present the results in units based on the short-range length scale r_0, i.e., length is in units of r_0 and energy in units of $1/mr_0^2$, where m is the mass of each identical particle.

B. Results

To illustrate the structure of the 2D three-body potentials and gain information about the collisional properties of the system, we have calculated the three-body potentials $U_\nu(R)$ for three identical bosons and three identical fermions for various values of $|M|_r^\pi$, with the results shown in Figs. 1 and 2. For these calculations, we assumed the interatomic interaction to be a pairwise sum of two-body interactions as shown in Eq. (9), where the two-body interaction is given by the short-range potential

$$v(r) = D\,\mathrm{sech}^2(r/r_0).\qquad(66)$$

Here, D is the potential depth and r_0 is the range of the interaction. This potential is known as the Pöschl-Teller potential [50]. The results in Figs. 1 and 2 were obtained for $D = -30/mr_0^2$, such that $v(r)$ supports three two-body bound states with total angular momentum $m_{2b} = 0$ (s wave), two with $|m_{2b}| = 1$ (p wave), one with $|m_{2b}| = 2$ (d wave), and
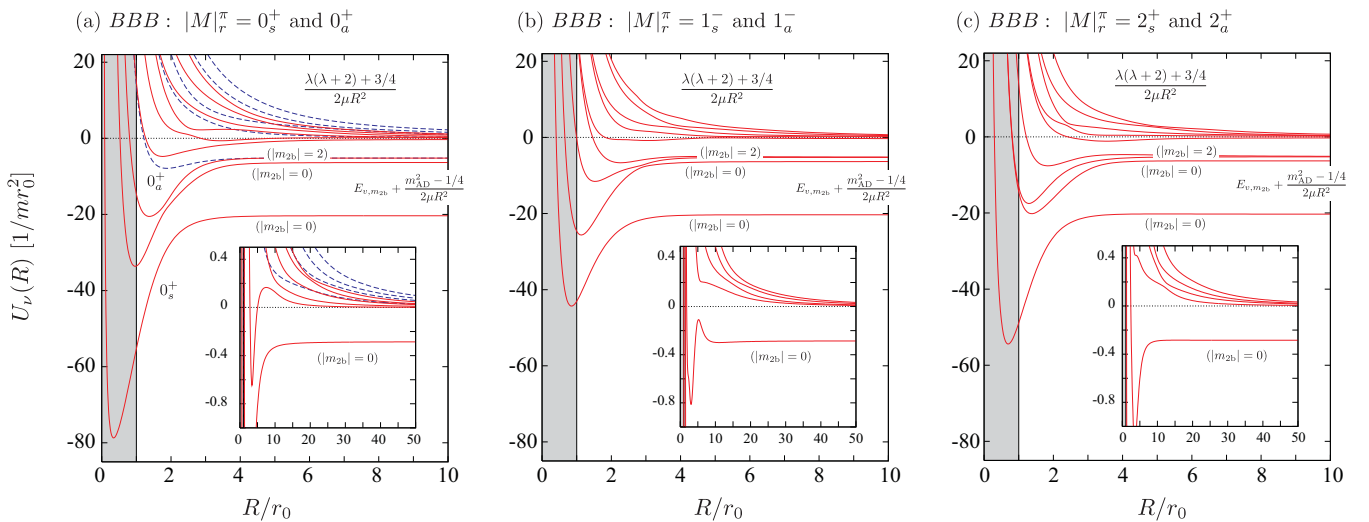

FIG. 1. (Color online) Three-body potentials for three identical bosons in 2D with (a) $|M|_r^\pi = 0_s^+$ (solid lines) and 0_a^+ (dashed lines), (b) $|M|_r^\pi = 1_s^-$ and 1_a^-, and (c) $|M|_r^\pi = 2_s^+$ and 2_a^+ (shaded region indicates the region in R in which particles can be found at distances smaller than the range of the interaction r_0). Note that for $|M| \neq 0$, the potentials for the symmetric and antisymmetric three-body systems (with respect to reflection) are exactly degenerate, while for $|M| = 0$ they are not. Note also that $m_{2b} = 0$ states are forbidden for the 0_a^+ symmetry in (a).
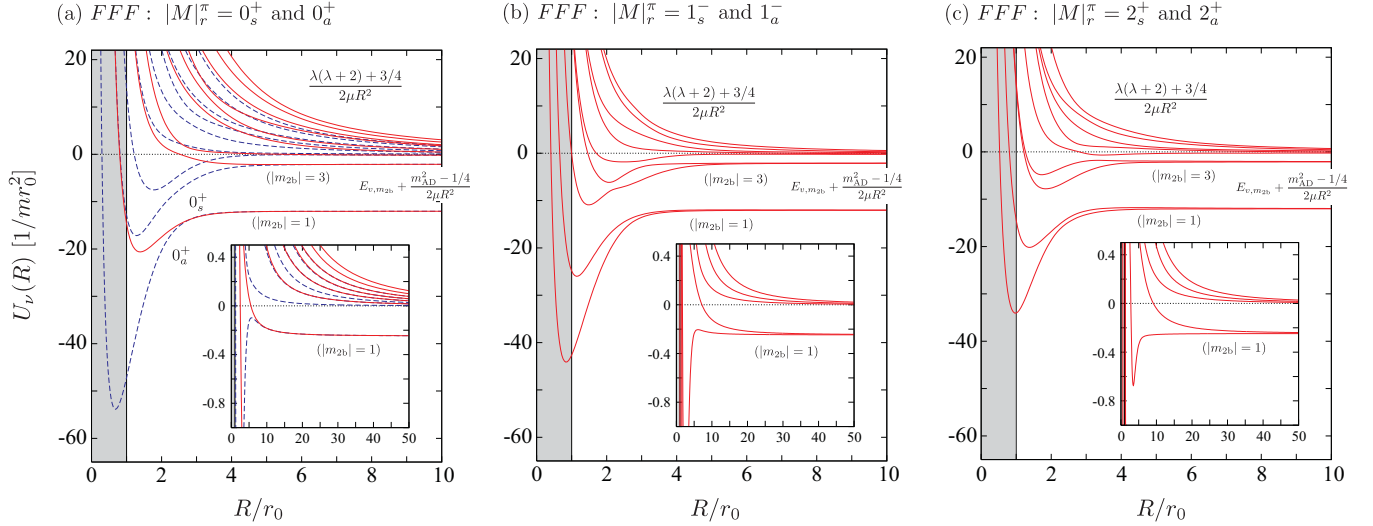
FIG. 2. (Color online) Three-body potentials for three identical fermions in 2D with (a) $|M|_r^\pi = 0_s^+$ (solid lines) and 0_a^+ (dashed lines), (b) $|M|_r^\pi = 1_s^-$ and 1_a^-, and (c) $|M|_r^\pi = 2_s^+$ and 2_a^+ (shaded region indicates the region R in which particles can be found at distances smaller than r_0). Note that, similar to identical bosons, the $|M| \neq 0$ potentials for the symmetric and antisymmetric 2D three-body systems (with respect to reflection) are exactly degenerate, while for $|M| = 0$ they are not.

one with $|m_{2b}| = 3$ (f wave). Note that for identical bosons the only states allowed by symmetry have m_{2b} even while identical fermions have m_{2b} odd. Note that our choice for D was made in order to produce nonresonant pairwise interactions.

Results for $|M| = 0$, 1, and 2 are given in Figs. 1 and 2 labeled by $|M|_r^\pi$, indicating the parity $\pi = (-1)^M$ as well as the reflection symmetry $r = s, a$ for symmetric and antisymmetric states, respectively. For states with $|M| \neq 0$, the symmetric and antisymmetric solutions $|M|_s^\pi$ and $|M|_a^\pi$ are exactly degenerate, which is equivalent to the degeneracy of $+M$ and $-M$. For $|M| = 0$ states [see Figs. 1(a) and 2(a)], however, the 0_s^+ and 0_a^+ states are nondegenerate and possess distinct properties for both bound and scattering states. Such differences, however, will become more clear below once we discuss the asymptotic behavior ($R \gg r_0$) of the three-body potentials. At these distances, two configurations for the three-body system are possible: three free particles (three-body continuum channels) and a diatom plus a free particle (atom-diatom channels).

C. Three-body continuum channels

As we saw in Sec. III, the motion of three free particles can be described in terms of hyperspherical harmonics [see Eqs. (18) and (19)]. Therefore, the leading-order behavior of the continuum channels is

$$W_\nu(R) \xrightarrow[R \to \infty]{} \frac{\lambda(\lambda + 2) + 3/4}{2\mu R^2}, \qquad (67)$$

with the allowed values for λ given in Tables I–IV in Sec. III. Our numerical results show that $Q_{\nu\nu}$ falls faster than $1/R^2$.

As mentioned above, $|M|_s^\pi$ and $|M|_a^\pi$ states with $M \neq 0$ are degenerate. For 0_s^+ and 0_a^+, however, the potentials are not degenerate, and the results in Tables I–IV include both symmetry states for $M = 0$. For instance, for three identical bosons, the $\lambda = 0$ solution is symmetric with respect to

reflection and is therefore a state of 0_s^+ symmetry. The lowest value of λ possible for $M = 0$ thus occurs for 0_s^+, and we will see that $\lambda_{\min}$ largely determines the low-energy behavior of scattering observables. For 0_a^+, $\lambda_{\min} = 8$. The opposite scenario holds for identical fermions where $\lambda_{\min} = 2$ for 0_a^+ while $\lambda_{\min} = 6$ for 0_s^+.

D. Atom-diatom channels

Asymptotically, W_ν for atom-diatom channels approaches the energy of the two-body bound states $E_{v,m_{2b}}$, v being the vibrational quantum number, with a leading $1/R^2$ behavior:

$$W_\nu(R) \xrightarrow[R \to \infty]{} E_{v,m_{2b}} + \frac{m_{AD}^2 - 1/4}{2\mu R^2}. \qquad (68)$$

Here, m_{AD} is the relative angular momentum between atom and diatom, satisfying $M = m_{2b} + m_{AD}$. For atom-diatom channels, the $-Q_{\nu\nu}/2\mu$ term is proportional to $1/R^2$, and its inclusion is crucial in order to properly recover W_ν at large distances since it exactly cancels an attractive term in W_ν. [Note that in Figs. 1 and 2 we show the numerical results for U_ν but label them with the expression for the asymptotic behavior of W_ν from Eqs. (67) and (68).]

For channels with $m_{2b} \neq 0$, two atom-diatom potentials converge to each threshold with $m_{AD} = M \mp |m_{2b}|$ corresponding to the $m_{2b} = \pm|m_{2b}|$ states. For $m_{2b} = 0$ states, of course, only $m_{AD} = M$ is allowed. These properties can be seen in the three-body potentials shown in Figs. 1(b) and 1(c) and Figs. 2(b) and 2(c). These statements must be qualified for the 0_s^+ and 0_a^+ curves in Figs. 1(a) and 2(a). Specifically, in Fig. 1(a), two-boson states with $m_{2b} = 0$ are not allowed for 0_a^+ since no reflection-antisymmetric solution can be constructed with $m_{2b} = 0$. Further, for both bosons and fermions with $m_{2b} \neq 0$, one of the two possible values of m_{AD} is of 0_s^+ symmetry, and the other is 0_a^+.

VI. THRESHOLD LAWS FOR INELASTIC COLLISIONS IN 2D

In this section, we determine the threshold laws [31], i.e., the low-energy dependence, of three-body scattering observables in 2D that are relevant for ultracold atoms. We have previously shown [31,34] that the energy dependence for inelastic scattering observables can be obtained by a simple WKB analysis and relies mostly on the asymptotic behavior of the initial potential relevant for the collision process. In fact, from Eqs. (67) and (68), we see that both atom-diatom and continuum channels can be written in terms of the familiar 3D centrifugal potential

$$W_\nu(R) \xrightarrow[R \to \infty]{} \frac{\ell_{\rm eff}(\ell_{\rm eff} + 1)}{2\mu R^2}, \tag{69}$$

with an effective angular momentum $\ell_{\rm eff}$ that depends on either λ or $m_{\rm AD}$. It is now straightforward to derive the threshold laws.

The energy dependence of scattering observables can be determined [34] from the observation that inelastic transitions occur at distances much smaller than the classical turning point r_c. In this case, the relevant transition probability $|T_{f \leftarrow i}|^2$ is proportional to the probability for all three particles to approach to such distances. We can thus approximate $|T_{f \leftarrow i}|^2$ using the WKB approximation for the tunneling probability from r_c to distances comparable to r_0,

$$|T_{f \leftarrow i}|^2 \propto \exp\left\{-2\int_{r_0}^{r_c} \sqrt{2\mu\left[W_i(R) + \frac{1/4}{2\mu R^2} - E\right]}dR\right\}. \tag{70}$$

In this expression, we have included the Langer correction [51] and will use Eq. (69) for $W_i(R)$. The turning point is then $r_c = (\ell_{\rm eff} + \frac{1}{2})/k$ with $k^2 = 2\mu E$. Therefore, in the WKB approximation, the energy dependence of the transition probability can be derived from the above integral, leading to

$$|T_{f \leftarrow i}|^2 \propto (kr_0)^{2\ell_{\rm eff}+1}, \tag{71}$$

with the value of $\ell_{\rm eff}$ determined from the symmetry of the system (through λ and $m_{\rm AD}$) as described in the previous sections.

We emphasize that our treatment here and the threshold laws in Eq. (71) assume that any corrections to Eq. (69) are sufficiently short ranged compared to R^{-2}. However, when there exists a weakly bound $m_{\rm 2b} = 0$ two-body state, it is not known what form the threshold laws will take. Equation (71) no longer applies since $m_{\rm 2b} = 0$ two-body states imply a large admixture of logarithm-containing terms in the low-energy two-body scattering state [7,8]. These, in turn, lead to logarithm-containing terms in $W_\nu(R)$ [19,20] that are not sufficiently short ranged compared to R^{-2}. For nonresonant interactions, however, our results should be valid. A more detailed study of the resonant case will be the subject of future analysis.
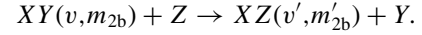
A. Atom-diatom collisions

In an ultracold mixture of atoms and molecules, the collisional processes primarily responsible for the mixture's stability are rovibrational relaxation

$$XY(v,m_{\rm 2b}) + Z \to XY(v',m'_{\rm 2b}) + Z,$$
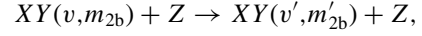
and reactive scattering

$$XY(v,m_{\rm 2b}) + Z \to XZ(v',m'_{\rm 2b}) + Y.$$

At ultracold temperatures, these reactions only occur if they are exothermic since the collision energy is generally orders of magnitude smaller than excitation energies. By the same token, the excitation energy released in these collisions as relative kinetic energy of the fragments is usually sufficient for the fragments to escape the trapping potential, thus leading to loss from the mixture. The energy dependence of both scattering processes, however, is the same as it only depends on the properties of the initial collision channel $XY(v,m_{\rm 2b}) + Z$.

For atom-diatom collisions, the initial collision channel is described at large distances by Eq. (68). Comparison with Eq. (69) allows us to identify $\ell_{\rm eff} = m_{\rm AD} - 1/2$. From Eq. (71) and the fact that the atom-diatom inelastic collision rate is proportional to $|T|^2$, we obtain

$$K_{\rm AD}^{(M)} \propto (k_{\rm AD}r_0)^{2|m_{\rm AD}|}, \tag{72}$$

where $k_{\rm AD}^2 = 2\mu_{\rm AD}(E - E_{v,m_{\rm 2b}})$ and $\mu_{\rm AD}$ is the atom-diatom reduced mass. The above expression is valid for energies smaller than the smallest energy scale in the system [52]. Therefore, if no other two-body state is more weakly bound than the diatom state, Eq. (72) should be valid for $k_{\rm AD}^2 \ll 2\mu_{\rm AD}|E_{v,m_{\rm 2b}}|$.

Equation (72) states that the threshold law is determined by the smallest value of $|m_{\rm AD}|$ allowed. Although it is not directly determined by identical particle symmetry, symmetry does indirectly influence it via $m_{\rm 2b}$ in $m_{\rm AD} = M \pm |m_{\rm 2b}|$. As we saw previously, for a given M and $m_{\rm 2b} = 0$ (s wave) only one value for $m_{\rm AD}$ is allowed, $m_{\rm AD} = M$. For $m_{\rm 2b} \neq 0$ two values for $m_{\rm AD}$ are allowed. We are interested, however, only on the lowest value for $|m_{\rm AD}|$, $|m_{\rm AD}| = ||M| - |m_{\rm 2b}||$ since it gives the dominant contribution to $K_{\rm AD}$ as $k_{\rm AD} \to 0$.

In Table VI, we summarize the threshold laws for the atom-diatom inelastic rate for all combinations of identical bosons and fermions for the lowest few values of $|M|$. Note that we use the 3D notation for angular momentum, i.e., $m_{\rm 2b} = 0,1,2,\ldots$ are represented by $s,p,d,\ldots$. Note also that for BBX systems, even values of $m_{\rm 2b}$ can be attributed either to a BB or BX molecule, while if $m_{\rm 2b}$ is odd it only can be attributed to a BX diatom. On the other hand, for FFX systems, even $m_{\rm 2b}$ can only be attributed to an FX diatom, while odd $m_{\rm 2b}$ can be either an FF or FX diatom. Based on these results, we can conclude that for any system the dominant partial wave (M) contribution to $K_{\rm AD}$ (see underlined results in Table VI) will be $|M| = |m_{\rm 2b}|$ and that $K_{\rm AD}$ is constant as $k_{\rm AD} \to 0$, even for identical fermions.

B. Three-body recombination

In ultracold atomic gases, three-body recombination

$$X + Y + Z \to XY + Z \tag{73}$$
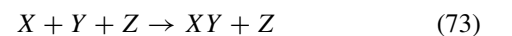
is often the major atom-loss mechanism since the atomic states are typically chosen to eliminate two-body collisional losses. The atom and diatom produced have large kinetic energy and

TABLE VI. Summary of the threshold laws for inelastic three-body processes in 2D for the lowest few values of $|M|_r^\pi$. Results are for atom-diatom inelastic rates (K_{AD}), three-body recombination (K_3), and collision-induced dissociation (D_3) for systems of three identical bosons (BBB), three identical fermions (FFF), two identical bosons (BBX), and two identical fermions (FFX), for both symmetric- and antisymmetric-reflection symmetries. The dominant partial wave contribution (M) is underlined for each system.

	$|M|_r^\pi$	$|m_{2b}|(|m_{AD}|)$	$K_{AD}^{(M)}$	λ_{min}	$K_3^{(M)}$	$D_3^{(M)}$
BBB	0_s^+	$s(0),d(2)$	$\underline{k_{AD}^0},k_{AD}^4$	0	$\underline{k^0}$	$\underline{k^2}$
	0_a^+	$d(2),g(4)$	k_{AD}^4,k_{AD}^8	8	k^{16}	k^{18}
	$1_{s/a}^-$	$s(1),d(1)$	k_{AD}^2,k_{AD}^2	3	k^6	k^8
	$2_{s/a}^+$	$s(2),d(0)$	$k_{AD}^4,\underline{k_{AD}^0}$	2	k^4	k^6
BBX	0_s^+	$s(0),p(1),d(2)$	$\underline{k_{AD}^0},k_{AD}^2,k_{AD}^4$	0	$\underline{k^0}$	$\underline{k^2}$
	0_a^+	$p(1),d(2),f(3)$	$k_{AD}^2,k_{AD}^4,k_{AD}^8$	4	k^8	k^{10}
	$1_{s/a}^-$	$s(1),p(0),d(1)$	$k_{AD}^2,\underline{k_{AD}^0},k_{AD}^2$	1	k^2	k^4
	$2_{s/a}^+$	$s(2),p(1),d(0)$	$k_{AD}^4,k_{AD}^2,\underline{k_{AD}^0}$	2	k^4	k^6
FFF	0_s^+	$p(1),f(3)$	k_{AD}^2,k_{AD}^6	6	k^{12}	k^{14}
	0_a^+	$p(1),f(3)$	k_{AD}^2,k_{AD}^6	2	$\underline{k^4}$	$\underline{k^6}$
	$1_{s/a}^-$	$p(0),f(2)$	$\underline{k_{AD}^0},k_{AD}^4$	3	k^6	k^8
	$2_{s/a}^+$	$p(1),f(1)$	k_{AD}^2,k_{AD}^2	4	k^8	k^{10}
FFX	0_s^+	$s(0),p(1),d(2)$	$\underline{k_{AD}^0},k_{AD}^2,k_{AD}^4$	2	k^4	k^6
	0_a^+	$p(1),d(2),f(3)$	$k_{AD}^2,k_{AD}^4,k_{AD}^8$	2	k^4	k^6
	$1_{s/a}^-$	$s(1),p(0),d(1)$	$k_{AD}^2,\underline{k_{AD}^0},k_{AD}^2$	1	$\underline{k^2}$	$\underline{k^4}$
	$2_{s/a}^+$	$s(2),p(1),d(0)$	$k_{AD}^4,k_{AD}^2,\underline{k_{AD}^0}$	2	k^4	k^6

are thus lost from the trap. In general, calculating three-body recombination rates requires the infinity of initial continuum channels [Eq. (67)], making the calculations extremely challenging. Fortunately, at ultracold collision energies, the lowest continuum channel provides the dominant contribution. This simplification allows us to apply the WKB approach above by identifying $\ell_{eff} = \lambda + 1/2$, leading to

$$K_3^{(M)} \propto k^{2\lambda} r_0^{2\lambda+2} \qquad (74)$$

for the three-body recombination rate $K_3 \propto |T|^2/k^2$, where $k^2 = 2\mu E$. This result is also expected to be valid for energies much smaller than any other energy scale in the system [52]. Therefore, Eq. (74) shows that for a given M, the dominant channel is determined by $\lambda = \lambda_{min}$.

Table VI includes the three-body recombination threshold laws for all combinations of identical particles. The dominant partial wave contribution, i.e., the one that has the lowest value for λ_{min}, is underlined in Table VI. For instance, for bosonic systems BBB and BBX, $M = 0$ is dominant with $\lambda_{min} = 0$, implying that K_3 is constant for $E \to 0$. For FFF systems, the dominant contribution is still $M = 0$, but with $\lambda_{min} = 2$ giving $K_3 \propto k^4$. For FFX systems, $M = 1$ dominates with $\lambda_{min} = 1$ for $K_3 \propto k^2$.

We note that for three identical bosons near an $m_{2b} = 0$ resonance, Ref. [20] found K_3 to vanish in the limit of $E \to 0$. The most likely explanation of this disagreement with the present analysis is that the logarithmic terms in $W_\nu(R)$

mentioned above do indeed have a dramatic effect on the threshold laws.

C. Collision-induced dissociation

The time reverse of three-body recombination, collision-induced dissociation

$$XY + Z \to X + Y + Z \qquad (75)$$
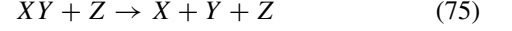
is only allowed if the collision energy is greater than the diatom binding energy such that the dissociation channels (three-body continuum channels) are energetically accessible. Therefore, at ultracold temperatures only dissociation of weakly bound molecules is possible. Because the collision-induced dissociation rate D_3 behaves as $D_3 \propto (kr_0)^{2\lambda+2}(k_{AD}r_0)^{2|m_{AD}|}$, it is the final three-body continuum channel that determines the threshold law since k_{AD} is finite at the breakup threshold where $k = 0$. The threshold law thus simplifies to

$$D_3^{(M)} \propto (kr_0)^{2\lambda+2}. \qquad (76)$$

We note that the energy dependence for D_3 differs from the one for K_3 by a factor k^2 due to the difference in phase-space factors from the reversed roles of the initial and final states. The D_3 threshold laws are also summarized in Table VI.

VII. SUMMARY

We have explored three-body systems in two dimensions using the adiabatic hyperspherical representation. We derived symmetry properties and boundary conditions for all permutation symmetries, establishing an efficient numerical approach for solving three-body problems in 2D. From explicit numerical examples, we demonstrated the asymptotic behavior of the three-body potentials and illustrated the topology of such potentials. From this analysis, complemented by our symmetry considerations, we were able to determine the threshold laws for atom-diatom inelastic collisions, as well as three-body recombination and collision-induced dissociation for various partial waves and symmetries. These results can be used for determining the expected collisional behavior and stability of ultracold atomic and molecular gases in two dimensions. The hyperspherical formalism we outline in this work is capable of treating three-body systems in which the two-body interactions can support deeply bound states as well as weakly bound states. Thus, in contrast to the formalisms in which a zero-range model potential is used, our approach is suitable for studying more realistic systems where the finite range aspect of the interatomic interactions plays an important rule.

ACKNOWLEDGMENTS

APPENDIX: EFFECTS OF SYMMETRY OPERATORS

To understand the effects of the symmetry operators, it is simplest to draw pictures of the mass-weighted Jacobi vectors
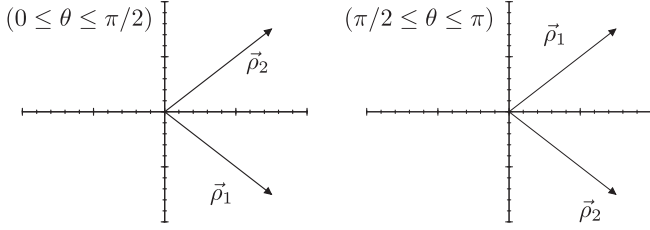
FIG. 3. Relation of the coordinate θ to the relative positions of the Jacobi vectors in the body frame.

in the center-of-mass frame. It is also necessary to understand the role of the coordinate θ. The essential point is illustrated in Fig. 3 which shows that the value of θ indicates the relative positions of the two Jacobi vectors.

The general scheme will then be to draw the Jacobi vectors, then draw the vectors resulting from the symmetry operation. The changes to the coordinates will be inferred from comparing the figures.

Because we do not change the moments of inertia with these symmetry operations, the body frame x and y axes can at most be inverted since they are defined from the Jacobi vectors. Consequently, γ can only be changed by 0 or π. It helps to know the moments of inertia:

$$I_{xx} = R^2 \sin^2\left(\frac{\theta}{2} - \frac{\pi}{4}\right), \tag{A1}$$

$$I_{yy} = R^2 \cos^2\left(\frac{\theta}{2} - \frac{\pi}{4}\right). \tag{A2}$$

For the same reason, θ can only be changed to $\pi - \theta$, if it is changed at all. This fact has the convenient consequence that we can pick a particular θ to work with and know that our results work for all θ. Thus, we will pick $\theta = 0$ (equilateral triangle) so that $\vec{\rho}_1$ is orthogonal to $\vec{\rho}_2$. This choice also produces a particularly simple form for the coordinates:

$$\begin{pmatrix} \rho_{2x}^L & \rho_{1x}^L \\ \rho_{2y}^L & \rho_{1y}^L \end{pmatrix} = \frac{R}{\sqrt{2}} \begin{pmatrix} \cos(\gamma + \varphi') & \sin(\gamma + \varphi') \\ \sin(\gamma + \varphi') & -\cos(\gamma + \varphi') \end{pmatrix} \tag{A3}$$

for $\theta = 0$, and

$$\begin{pmatrix} \rho_{2x}^L & \rho_{1x}^L \\ \rho_{2y}^L & \rho_{1y}^L \end{pmatrix} = \frac{R}{\sqrt{2}} \begin{pmatrix} \cos(\gamma - \varphi') & -\sin(\gamma - \varphi') \\ \sin(\gamma - \varphi') & \cos(\gamma - \varphi') \end{pmatrix} \tag{A4}$$

for $\theta = \pi$. Given the coordinates' dependence on θ and φ [see Eq. (4)], in what follows it is simpler to work with $\theta' = \left(\frac{\theta}{2} - \frac{\pi}{4}\right)$ and $\varphi' = \left(\frac{\varphi}{2} + \frac{\pi}{6}\right)$. The coordinate φ' just measures the angle of $\vec{\rho}_2$ from the x axis and takes on values between $\frac{\pi}{6}$ and $\frac{7\pi}{6}$. Nevertheless, our results will finally be expressed in terms of θ and φ. Note that we found we had to be careful to split each operation up over two intervals in φ [45]. Not too surprisingly, it turns out that even though the coordinates are affected differently in the two intervals, the functions that depend on them are not. This property allows us to obtain the single expression for each operator shown in Eqs. (20)–(25), valid over the whole range of φ.
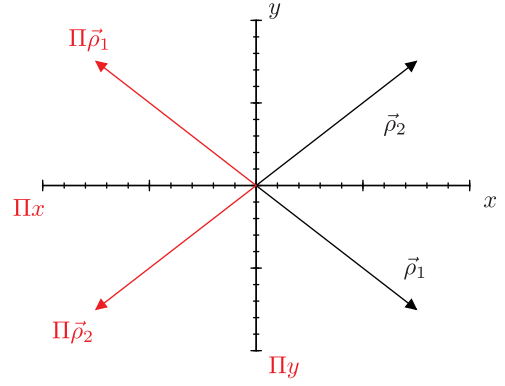

FIG. 4. (Color online) Jacobi vectors before (black) and after (red) the parity operation Π.

1. Parity

The parity operation has the following effects on the mass-scaled Jacobi vectors,

$$\Pi(\vec{\rho}_1, \vec{\rho}_2) = (-\vec{\rho}_1, -\vec{\rho}_2). \tag{A5}$$

This operation is illustrated in Fig. 4. Now, using Eq. (4) of the main text, we find that the hyperspherical coordinates are affected by parity operation as

$$\Pi(\theta, \varphi, \gamma) = (\theta, \varphi, \pi + \gamma). \tag{A6}$$

As a consequence, it is easy to determine that the hyperspherical harmonics [Eq. (19)] are affected by parity as

$$\Pi Y_{\omega M}^\lambda(\Omega) = (-1)^M Y_{\omega M}^\lambda(\Omega), \tag{A7}$$

where $\Omega \equiv \{\theta, \varphi, \gamma\}$.

2. Permutation: P_{12}

Choosing $\vec{\rho}_1$ as the Jacobi vector connecting particles 1 and 2, P_{12} has the following effect,

$$P_{12}(\vec{\rho}_1, \vec{\rho}_2) = (-\vec{\rho}_1, \vec{\rho}_2) \tag{A8}$$

as illustrated in Fig. 5.

First, since the relative positions of $\vec{\rho}_1$ and $\vec{\rho}_2$ have changed in the sense of Fig. 3, we know $P_{12}\theta' = -\theta'$ ($P_{12}\theta = \pi - \theta$). As a consequence, $P_{12}\varphi'$ increases in the direction opposite
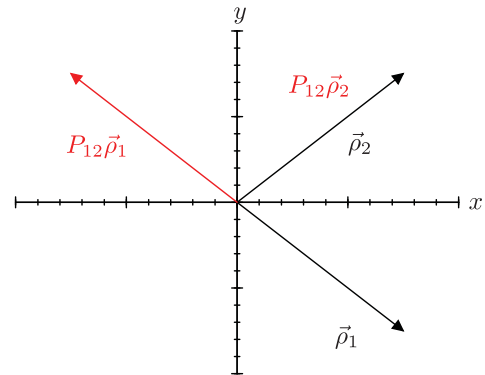

FIG. 5. (Color online) Jacobi vectors before (black) and after (red) the P_{12} permutation operation.
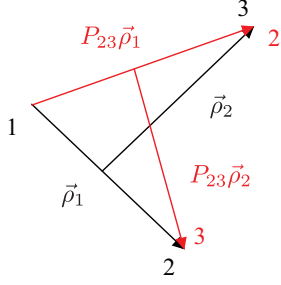
FIG. 6. (Color online) Jacobi vectors before (black) and after (red) the P_{23} permutation operation.

to φ', i.e., $P_{12}\varphi'$ increases clockwise while φ' increases counterclockwise [see Eqs. (A3) and (A4)]. Second, since $P_{12}\varphi'$ has the same range as φ', we must make sure that both stay within this range. After some head scratching and careful drawing, we find the following:

$$P_{12}(\theta',\varphi',\gamma) = \begin{cases} (-\theta',\pi - \varphi',\pi + \gamma) & \text{for } \frac{\pi}{6} \leqslant \varphi' \leqslant \frac{5\pi}{6}, \\ (-\theta',2\pi - \varphi',\gamma) & \text{for } \frac{5\pi}{6} \leqslant \varphi' \leqslant \frac{7\pi}{6}. \end{cases}$$
(A9)

Note that both of these branches give the same value of $\gamma - \varphi'$ consistent with Eq. (A4). This will be true for all the P_{ij}. Converting to the original coordinates gives

$$P_{12}(\theta,\varphi,\gamma) = \begin{cases} (\pi - \theta,\frac{4\pi}{3} - \varphi,\pi + \gamma) & \text{for } 0 \leqslant \varphi \leqslant \frac{4\pi}{3}, \\ (\pi - \theta,\frac{10\pi}{3} - \varphi,\gamma) & \text{for } \frac{4\pi}{3} \leqslant \varphi \leqslant 2\pi. \end{cases}$$
(A10)

Now, from Eq. (19) and using $d_{mm'}^{\ell}(\pi - \theta) = (-1)^{\ell+m'}d_{-mm'}^{\ell}(\theta)$ and Eq. (11), one can show that the effect of the permutation P_{12} on the hyperspherical harmonics does not depend on the range in φ and is given by

$$P_{12}Y_{\omega M}^{\lambda}(\Omega) = (-1)^{\frac{M+\lambda}{2}}e^{-i\omega\frac{\pi}{3}}Y_{-\omega M}^{\lambda}(\Omega).$$
(A11)

3. Permutation: P_{23}

For this operation, we could write out the explicit changes in $\vec{\rho}_1$ and $\vec{\rho}_2$, but we believe it is easier to just draw the vectors illustrating the effect of P_{23} as shown in Fig. 6.

We should now make a drawing like Fig. 5, but hopefully the idea is getting clear. The key is to realize that since the particles are in an equilateral configuration, the angle between $P_{23}\vec{\rho}_1$ and $\vec{\rho}_1$ is $\frac{\pi}{3}$. We similarly know all of the other relative angles, and they are simple, which is why we chose to work

with $\theta = 0$. We find

$$P_{23}(\theta',\varphi',\gamma) = \begin{cases} (-\theta',\frac{2\pi}{3} - \varphi',\gamma) & \text{for } \frac{\pi}{6} \leqslant \varphi' \leqslant \frac{\pi}{2}, \\ (-\theta',\frac{5\pi}{3} - \varphi',\pi + \gamma) & \text{for } \frac{\pi}{2} \leqslant \varphi' \leqslant \frac{7\pi}{6} \end{cases}$$
(A12)

or

$$P_{23}(\theta,\varphi,\gamma) = \begin{cases} (\pi - \theta,\frac{2\pi}{3} - \varphi,\gamma) & \text{for } 0 \leqslant \varphi \leqslant \frac{2\pi}{3}, \\ (\pi - \theta,\frac{8\pi}{3} - \varphi,\pi + \gamma) & \text{for } \frac{2\pi}{3} \leqslant \varphi \leqslant 2\pi. \end{cases}$$
(A13)

Similar to P_{12}, one can show that the effect of P_{23} does not depend on the range in φ and is given by

$$P_{23}Y_{\omega M}^{\lambda}(\Omega) = (-1)^{\frac{M+\lambda}{2}}e^{i\omega\frac{\pi}{3}}Y_{-\omega M}^{\lambda}(\Omega).$$
(A14)

4. Permutations P_{31}, $P_{12}P_{23}$, and $P_{12}P_{31}$

Making drawings like Figs. 5 and 6, it is possible to derive the effect of the permutations P_{31}, $P_{12}P_{23}$, and $P_{12}P_{31}$. Note that these effects could be worked out from the P_{12} and P_{23}, but because of the different ranges for φ, this approach would be complicated. We will forego more figures, however, and simply state the results for the remaining permutations and corresponding actions on the hyperspherical harmonics.

For P_{31} the result is particularly simple (the range of φ is not split),

$$P_{31}(\theta,\varphi,\gamma) = (\pi - \theta,2\pi - \varphi,\gamma),$$
(A15)

which leads to

$$P_{31}Y_{\omega M}^{\lambda}(\Omega) = (-1)^{\frac{M+\lambda}{2}}e^{i\omega\pi}Y_{-\omega M}^{\lambda}(\Omega).$$
(A16)

For $P_{12}P_{31}$ and $P_{12}P_{23}$, we obtain

$$P_{12}P_{31}(\theta,\varphi,\gamma) = \begin{cases} (\theta,\frac{2\pi}{3} + \varphi,\pi + \gamma) & \text{for } 0 \leqslant \varphi \leqslant \frac{4\pi}{3}, \\ (\theta,-\frac{4\pi}{3} + \varphi,\gamma) & \text{for } \frac{4\pi}{3} \leqslant \varphi \leqslant 2\pi \end{cases}$$
(A17)

and

$$P_{12}P_{23}(\theta,\varphi,\gamma)$$
$$= \begin{cases} (\theta,\frac{4\pi}{3} + \varphi,\gamma) & \text{for } 0 \leqslant \varphi \leqslant \frac{2\pi}{3}, \\ (\theta,-\frac{2\pi}{3} + \varphi,\pi + \gamma) & \text{for } \frac{2\pi}{3} \leqslant \varphi \leqslant 2\pi. \end{cases}$$
(A18)

These, therefore, lead to

$$P_{12}P_{31}Y_{\omega M}^{\lambda}(\Omega) = e^{-i\omega\frac{2\pi}{3}}Y_{\omega M}^{\lambda}(\Omega),$$
(A19)

$$P_{12}P_{23}Y_{\omega M}^{\lambda}(\Omega) = e^{i\omega\frac{2\pi}{3}}Y_{\omega M}^{\lambda}(\Omega).$$
(A20)

[1] C. Chin, R. Grimm, P. Julienne, and E. Tiesinga, Rev. Mod. Phys. **82**, 1225 (2010).

[2] E. Braaten and H.-W. Hammer, Phys. Rep. **428**, 259 (2006).

[3] Y. Wang, J. P. D'Incao, and B. D. Esry, Adv. At. Mol. Opt. Phys. **62**, 1 (2013).

[4] Y. Wang, J. P. D'Incao, and C. H. Greene, Phys. Rev. Lett. **106**, 233201 (2011).

[5] Y. Wang, J. P. D'Incao, and C. H. Greene, Phys. Rev. Lett. **107**, 233201 (2011).

[6] N. L. Guevara, Y. Wang, and B. D. Esry, Phys. Rev. Lett. **108**, 213202 (2012).

[7] S.-M. Shih and D.-W. Wang, Phys. Rev. A **79**, 065603 (2009).

[8] K. Kanjilal and D. Blume, Phys. Rev. A **73**, 060701(R) (2006).

[9] E. Nielsen, D. V. Fedorov, A. S. Jensen, and E. Garrido, Phys. Rep. **347**, 373 (2001).

[10] D. S. Petrov and G. V. Shlyapnikov, Phys. Rev. A **64**, 012706 (2001).

[11] X.-J. Liu, H. Hu, and P. D. Drummond, Phys. Rev. B **82**, 054524 (2010).

[12] L. W. Bruch and J. A. Tjon, Phys. Rev. A **19**, 425 (1979).

[13] E. Nielsen, D. V. Fedorov, and A. S. Jensen, Few-Body Syst. **27**, 15 (1999).

[14] L. Platter, H.-W. Hammer, and U.-G. Meißner, Few-Body Syst. **35**, 169 (2004).

[15] H.-W. Hammer and D. T. Son, Phys. Rev. Lett. **93**, 250408 (2004).

[16] D. Blume, Phys. Rev. B **72**, 094510 (2005).

[17] I. V. Brodsky, M. Yu. Kagan, A. V. Klaptsov, R. Combescot, and X. Leyronas, Phys. Rev. A **73**, 032724 (2006).

[18] D. Lee, Phys. Rev. A **73**, 063204 (2006).

[19] O. I. Kartavtsev and A. V. Malykh, Phys. Rev. A **74**, 042506 (2006).

[20] K. Helfrich and H.-W. Hammer, Phys. Rev. A **83**, 052703 (2011).

[21] F. F. Bellotti, T. Frederico, M. T. Yamashita, D. V. Fedorov, A. S. Jensen, and N. T. Zinner, J. Phys. B: At., Mol. Opt. Phys. **44**, 205302 (2011).

[22] F. F. Bellotti, T. Frederico, M. T. Yamashita, D. V. Fedorov, A. S. Jensen, and N. T. Zinner, Phys. Rev. A **85**, 025601 (2012).

[23] F. F. Bellotti, T. Frederico, M. T. Yamashita, D. V. Fedorov, A. S. Jensen, and N. T. Zinner, J. Phys. B: At., Mol. Opt. Phys. **46**, 055301 (2013).

[24] Y. Nishida, S. Moroz, and D. T. Son, Phys. Rev. Lett. **110**, 235301 (2013).

[25] A. G. Volosniev, D. V. Fedorov, A. S. Jensen, and N. T. Zinner, J. Phys. B: At., Mol. Opt. Phys. **47**, 185302 (2014).

[26] Y. Nishida and S. Tan, Phys. Rev. A **79**, 060701(R) (2009).

[27] Y. Nishida and S. Tan, Phys. Rev. A **82**, 062713 (2010).

[28] Y. Nishida, Phys. Rev. A **82**, 011605(R) (2010).

[29] G. Lamporesi, J. Catani, G. Barontini, Y. Nishida, M. Inguscio, and F. Minardi, Phys. Rev. Lett. **104**, 153202 (2010).

[30] E. Haller, M. J. Mark, R. Hart, J. G. Danzl, L. Reichsöllner, V. Melezhik, P. Schmelcher, and H.-C. Nägerl, Phys. Rev. Lett. **104**, 153203 (2010).

[31] B. D. Esry, C. H. Greene, and H. Suno, Phys. Rev. A **65**, 010705 (2001).

[32] E. Nielsen and J. H. Macek, Phys. Rev. Lett. **83**, 1566 (1999).

[33] B. D. Esry, C. H. Greene, and J. P. Burke Jr., Phys. Rev. Lett. **83**, 1751 (1999).

[34] J. P. D'Incao and B. D. Esry, Phys. Rev. Lett. **94**, 213201 (2005).

[35] C. D. Lin, Phys. Rep. **257**, 1 (1995).

[36] F. T. Smith, J. Math. Phys. **3**, 735 (1962).

[37] R. C. Whitten and F. T. Smith, J. Math. Phys. **9**, 1103 (1968).

[38] B. R. Johnson, J. Chem. Phys. **73**, 5051 (1980).

[39] B. Lepetit, Z. Peng, and A. Kuppermann, Chem. Phys. Lett. **166**, 572 (1990).

[40] B. K. Kendrick, R. T. Pack, R. B. Walker, and E. F. Hayes, J. Chem. Phys. **110**, 6673 (1999).

[41] H. Suno, B. D. Esry, C. H. Greene, and J. P. Burke Jr., Phys. Rev. A **65**, 042725 (2002).

[42] H. Suno and B. D. Esry, Phys. Rev. A **82**, 062521 (2010).

[43] H. Suno and B. D. Esry, Phys. Rev. A **78**, 062701 (2008).

[44] H. Suno and B. D. Esry, Phys. Rev. A **80**, 062702 (2009).

[45] B. R. Johnson, J. Chem. Phys. **79**, 1916 (1983).

[46] L. M. Delves, Nucl. Phys. **9**, 391 (1958); **20**, 275 (1960).

[47] J. P. D'Incao, C. H. Greene, and B. D. Esry, J. Phys. B: At., Mol. Opt. Phys. **42**, 044016 (2009).

[48] M. Hamermesh, *Group Theory and its Application to Physical Problems* (Dover, New York, 1989).

[49] C. de Boor, *A Practical Guide to Splines* (Springer, New York, 1978).

[50] L. D. Landau and E. M. Lifshitz, *Quantum Mechanics: Non-Relativistic Theory* (Butterworth-Heinemann, London, 1981).

[51] M. V. Berry and K. E. Mount, Rep. Prog. Phys. **35**, 315 (1972).

[52] J. P. D'Incao, H. Suno, and B. D. Esry, Phys. Rev. Lett. **93**, 123201 (2004).